

Modeling of solvent flow effects in enzyme catalysis under physiological conditions

Jeremy Schofield, Paul Inder, and Raymond Kapral

Citation: *J. Chem. Phys.* **136**, 205101 (2012); doi: 10.1063/1.4719539

View online: <http://dx.doi.org/10.1063/1.4719539>

View Table of Contents: <http://jcp.aip.org/resource/1/JCPSA6/v136/i20>

Published by the [American Institute of Physics](#).

Additional information on J. Chem. Phys.


Journal Homepage: <http://jcp.aip.org/>

Journal Information: http://jcp.aip.org/about/about_the_journal

Top downloads: http://jcp.aip.org/features/most_downloaded

Information for Authors: <http://jcp.aip.org/authors>

ADVERTISEMENT



AIPAdvances

Special Topic Section:
PHYSICS OF CANCER

Why cancer? Why physics? [View Articles Now](#)

Modeling of solvent flow effects in enzyme catalysis under physiological conditions

Jeremy Schofield,^{a)} Paul Inder,^{b)} and Raymond Kapral^{c)}

Chemical Physics Theory Group, Department of Chemistry, University of Toronto, Toronto, Ontario M5S 3H6, Canada

(Received 13 March 2012; accepted 3 May 2012; published online 22 May 2012)

A stochastic model for the dynamics of enzymatic catalysis in explicit, effective solvents under physiological conditions is presented. Analytically-computed first passage time densities of a diffusing particle in a spherical shell with absorbing boundaries are combined with densities obtained from explicit simulation to obtain the overall probability density for the total reaction cycle time of the enzymatic system. The method is used to investigate the catalytic transfer of a phosphoryl group in a phosphoglycerate kinase-ADP-bis phosphoglycerate system, one of the steps of glycolysis. The direct simulation of the enzyme-substrate binding and reaction is carried out using an elastic network model for the protein, and the solvent motions are described by multiparticle collision dynamics which incorporates hydrodynamic flow effects. Systems where solvent-enzyme coupling occurs through explicit intermolecular interactions, as well as systems where this coupling is taken into account by including the protein and substrate in the multiparticle collision step, are investigated and compared with simulations where hydrodynamic coupling is absent. It is demonstrated that the flow of solvent particles around the enzyme facilitates the large-scale hinge motion of the enzyme with bound substrates, and has a significant impact on the shape of the probability densities and average time scales of substrate binding for substrates near the enzyme, the closure of the enzyme after binding, and the overall time of completion of the cycle. © 2012 American Institute of Physics. [<http://dx.doi.org/10.1063/1.4719539>]

I. INTRODUCTION

Biochemical reactions in the cell are often carried out through complex chemical networks consisting of many coupled elementary component steps.¹ Even the elucidation of the molecular-level mechanism, which underlies the operation of a single component in such networks is often a difficult task. Computer simulation is playing an increasingly important role in such mechanistic studies but direct simulation of many biochemical processes is challenging because they occur on a diverse range of scales. This fact has prompted the development of coarse-grain or mesoscopic methods that allow one to circumvent some of the difficulties related to dynamics that take place on long space and time scales.^{2,3} In enzyme kinetics long time scales can arise from the diffusive approach of the substrate to the enzyme and the conformational changes in the enzyme in the course of the catalytic reactions it carries out. There have been numerous simulation studies of the effects of diffusion on enzyme kinetics.^{4–8} In this paper, we describe how one may construct a mesoscopic model of an enzymatic cycle that incorporates the diffusive approach of substrates to the enzyme based on the solution of the diffusion equation, along with a particle-based description of the enzymatic reaction that involves protein conformational changes, release of the product, and the return of the protein to its original conformation.

The method is used to investigate a specific enzymatic reaction,



catalyzed by the enzyme phosphoglycerate kinase (PGK). This reaction is an important step in the glycolysis network. In particular, we focus on the forward reaction that involves the transfer of a phosphoryl group from 1,3-bisphosphoglycerate (bPG) to ADP by the PGK enzyme to form 3-phosphoglycerate (PG) and ATP. (Often it is the reverse reaction that is studied experimentally due to the instability of bPG.⁹) Phosphoglycerate kinase is a monomeric protein of moderate size (416 amino acid residues in the human isozyme studied here) found in all living organisms, with a highly conserved amino acid sequence across different life forms. Its structure, consisting of two equal-sized domains labeled by the N- and C-termini of the protein, is well adapted to selectively bind two substrates, bPG binds to the N-terminal, while the nucleotide substrates, MgATP or MgADP, bind to the C-terminal domain of the enzyme. Structurally, the N- and C-domains consist of a 6-stranded parallel beta sheet surrounded by alpha helices (see Fig. 1).

The mechanism for the enzymatic reaction, which involves large hinge-bending motions of the domains of the protein,^{10–12} has been the subject of many kinetic studies.^{9,13–15} The activity of the enzyme requires both substrates to be bound.^{11,16,17} When both substrates bind, the enzyme undergoes a large-scale hinge-bending conformational

^{a)}E-mail: jmschofi@chem.utoronto.ca.

^{b)}E-mail: pinder@chem.utoronto.ca.

^{c)}E-mail: rkapral@chem.utoronto.ca.

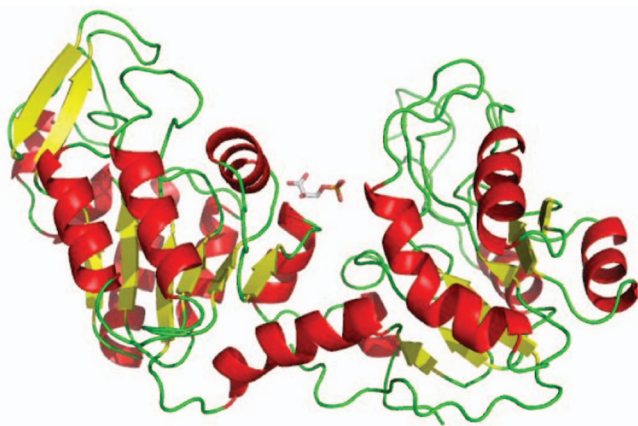


FIG. 1. The open conformation of phosphoglycerate kinase showing the (right) N- and (left) C-terminal domains of the protein. The N-terminal domain binds 3-phosphoglycerate and 1,3-bisphosphoglycerate, while the C-terminal domain binds MgATP and MgADP.

change that brings the substrates close to one another to catalyze the dephosphorylation of bPG. In this “closed” conformation, the transition state is stabilized, lowering the free energy barrier for the transfer of a phosphoryl group. Upon transfer, the enzyme is forced into an open configuration and the PG and ATP products are released.

We shall be concerned with the enzymatic activity of PGK under physiological conditions in the cell where the binding process is diffusion limited.¹⁸ The binding process is well suited to be modeled as a two-step process in which first the substrates diffuse freely into a region near the enzyme, and then are drawn into the binding sites on the enzyme. Thus, it is reasonable to utilize a hybrid, stochastic procedure that combines analytical calculations with explicit simulation. The first step in the process of computing the distribution of time scales of the catalytic activity of the enzyme can be estimated by calculating first-passage times for the substrates moving into the vicinity of the enzyme, while the second step requires a more detailed dynamical simulation due to the influence of the enzyme on the dynamics of the substrate. There have been simulations of the domain motions of PGK using a variety of methods.^{19–23} Given the large size of the protein and the long time scales of the motions, a full molecular dynamics (MD) simulation of the second step, which involves binding of the substrates to the enzyme in solution, the hinge-bending motion of the enzyme-substrate complex, followed by the reaction of the substrates and final release of products coupled with the re-opening of the enzyme, is computationally demanding. Consequently, we develop a coarse-grain description of this part of the enzymatic cycle that is particle-based, includes enzyme, substrates, and solvent molecules explicitly and retains many features of full molecular dynamics.

The outline of the paper is as follows. The two steps of the enzymatic reaction dynamics, diffusive approach of enzyme and substrate and substrate binding and reaction, are described first. The mesoscopic model for the protein, substrates, and solvent, along with a description of the interaction potentials that control the binding of the bPG substrate to the active site and conformational changes in the PGK pro-

tein, are the topics of Sec. II. Section III discusses the various time scales involved in the diffusive encounter between the substrates and the enzyme and shows how the relevant first-passage times can be computed analytically. The results of simulations of the dynamics are reported in Sec. IV while the conclusions of the study are summarized in Sec. V.

II. PROTEIN AND ITS CATALYTIC ACTIVITY IN SOLUTION

We consider a system containing PGK enzymes, along with substrate and solvent molecules. The enzyme exists in open and closed forms and binding of both substrates is necessary for large-scale conformational changes to occur.^{12,15,17} We suppose that the ADP substrate is bound to the enzyme and construct a coarse-grain model of the protein interacting with the bPG substrate in the presence of solvent. As discussed below, under physiological conditions, ADP binds quickly and the rate of the enzymatic reaction is determined by the binding of bPG. The model of the enzymatic activity of PGK entails a description of the interactions of bPG with the enzyme as it binds to the active site, the conformational changes in the protein that lead to the reactive event and the release of product and return of the protein to its original conformation.

A. Network model of PGK and interactions with substrate

A coarse-grain network model of the PGK protein is constructed by replacing each amino acid residue with a single monomer bead and connecting the beads by links or bonds.^{3,24–26} The bound ADP substrate is treated as one of the protein beads, while the bPG substrate is also described in a coarse-grained fashion as a single bead. The set of bead coordinates $\mathbf{R}^{N_p} = (\mathbf{R}_1, \mathbf{R}_2, \dots, \mathbf{R}_{N_p})$ specifies the configuration of the protein (P) and we let \mathbf{R} denote the coordinate of bPG, henceforth called the substrate (S). The construction of the potential energy function that is responsible for the protein conformational state and interactions between the protein and substrate is described in detail in Appendix A. Here, we simply sketch the main elements that enter in the design of the potential function, $V_{PS}(\mathbf{R}^{N_p}, \mathbf{R}; \xi)$, that is able to describe both conformational states of the protein, the binding of bPG to the active site, and the resulting changes of protein conformational states that occur on substrate binding and product release.²⁷

To construct a network model for PGK, protein database configurations built from crystallographic data were analyzed to determine a set of pairwise interactions between residues. Each of the 416 residues was represented by a single monomer bead in a linear polymer representation of the protein, with the position of each bead taken to be the Cartesian coordinates of the alpha carbon of the peptide. Both open and closed forms of the PGK molecule were taken from the initial and final protein database configurations generated from the morphing analysis of the conformational change between open and closed conformations^{28,29} in the database of macromolecular movements.³⁰

Pairs of beads separated by a distance $r < 10 \text{ \AA}$ were recorded, generating separate lists of indices for open and closed conformations. The interaction lists for open and closed configurations were then compared, and a set \mathcal{B}_c of common interaction pairs or links were identified and assigned bond potentials in the following way. For links in \mathcal{B}_c the bond length as well as the magnitude of the difference r_{co} between the bond lengths in the open and closed conformations were computed. The links in \mathcal{B}_c were then grouped into two new subsets, \mathcal{B}_{hc} and \mathcal{B}_{sc} , containing hard- (hc) or soft-common (sc) links, respectively, based on the value of the separation distance r_{co} , where links with $r_{co} < 4$ were identified as hard links. The list of common links was then compared with the lists of open links and closed links. This process yielded 2891 hard-common links and 519 soft-common links. In this study, the ADP substrate is treated as a single bead that forms hard links with three different beads in the enzyme.

Pairs that exist in either the list of open links or the list of closed links but not in both were sorted into soft-open, \mathcal{B}_{so} , and soft-closed, \mathcal{B}_{sx} sets, respectively. There are 448 soft-open links (so), and 619 soft-closed links (sx).

Before the enzymatic reaction can occur, bPG must bind to the active site of the enzyme. The binding pocket of the enzyme for this substrate was defined by beads with coordinates $(\mathbf{R}_0^a, \mathbf{R}_1^a, \mathbf{R}_2^a)$, where \mathbf{R}_0^a , \mathbf{R}_1^a , and \mathbf{R}_2^a are the coordinates of the alpha carbon of the glycine residues 386, 387, and 388 in the amino acid sequence of the PGK enzyme. The binding interaction between the bPG substrate at position \mathbf{R} and the enzyme was assumed to depend on both the distance between the substrate and the bead in the active site with coordinate \mathbf{R}_1^a , $|\mathbf{R} - \mathbf{R}_1^a| = R_{S1}$, as well as the orientation of the substrate with respect to a coordinate frame determined by three beads defining the binding pocket of the enzyme. As the substrate binds it triggers conformational changes in the protein that lead to hinge closing to bring the bPG and ADP substrates into proximity for the phosphoryl group transfer. Consequently, as bPG interacts with the protein in the course of binding to the active site, the open protein configuration is destabilized with respect to the closed configurations, driving the enzyme towards the closed conformation. To achieve this conformational change, the interaction potentials for the soft, non-common set of links were taken to depend on a reaction coordinate $\xi(R_{S1})$, which is a function of the distance between bPG and the active site. The net effect of the combination of these contributions is a protein-substrate interaction potential, $V_{PS}(\mathbf{R}^{N_p}, \mathbf{R}; \xi)$, which can draw in the bPG substrate, bind it to the active site of the enzyme in the open configuration, and then cause the enzyme to undergo a conformational change from an open to closed configuration. The network model of the protein and the binding of the substrate to the open conformation leading to hinge closing is shown in Fig. 2. After binding has taken place, the phosphoryl group transfer reaction is carried out by treating the reaction coordinate ξ as an external control parameter whose value is determined probabilistically. When the reaction is complete the closed configuration is unstable and the enzyme reopens, completing the cycle.

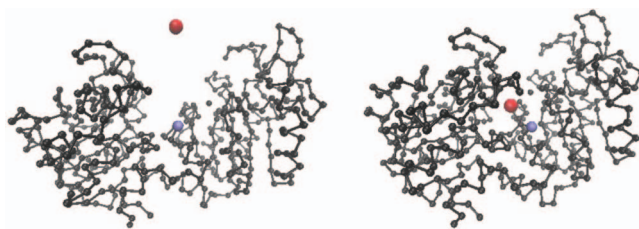


FIG. 2. (Left) Open conformation of the network model of PGK showing the approach of bPG to the binding pocket of the enzyme. (Right) Protein conformation after substrate binding has resulted in hinge closing to form the closed form.

B. Solvent and its interactions with the protein and substrate

The system also contains N_s solvent molecules with positions, $\mathbf{r}^{N_s} = (\mathbf{r}_1, \mathbf{r}_2, \dots, \mathbf{r}_{N_s})$ and velocities, $\mathbf{v}^{N_s} = (\mathbf{v}_1, \mathbf{v}_2, \dots, \mathbf{v}_{N_s})$. The solvent evolution is modeled by multiparticle collision (MPC) dynamics.³¹ In MPC dynamics there are no intermolecular potentials among solvent molecules. Instead, solvent molecules propagate in the absence of solvent-solvent interactions and undergo multiparticle collisions at discrete times τ that account for the effects of many real collisions during this time interval. More specifically, after the streaming step, solvent particles are assigned to cells with length ℓ for the purposes of carrying out multiparticle collisions. To ensure that the dynamics is Galilean invariant, uniform random grid-shifts are applied prior to the assignment of particles to cells.^{32,33} The center-of-mass velocity \mathbf{v}_c of particles in a cell is computed for each cell c , and the velocities of the solvent particles relative to the center-of-mass velocity are rotated around a uniformly chosen random Cartesian axis (x, y, or z) by an angle chosen from the set of angles, $\{\pm \pi/4, \pm \pi/2, \pm 3\pi/4\}$. Note that, other rules for the collision step can also be implemented without changing the character of the model or qualitative results in Sec. IV, though they might have a modest influence on the transport coefficients of the solvent. The collision step for a particle i in cell c is therefore,

$$\mathbf{v}'_i = \mathbf{v}_c + \boldsymbol{\omega} \cdot (\mathbf{v}_i - \mathbf{v}_c), \quad (2)$$

where \mathbf{v}'_i is the post-collision velocity of particle i and $\boldsymbol{\omega}$ is a rotation matrix. Multiparticle collision dynamics conserves linear momentum, energy, and particle number, and is consistent with hydrodynamic flow.^{34,35} Although this collision rule does not locally conserve angular momentum, this can be rectified at some increase in computational cost.³⁶ Since our system is initially at equilibrium and free of rotational motion and external forces or torques the more elaborate collision rule is not required in this study.

When the system contains proteins and substrates dissolved in the solvent, the evolution is described by hybrid MD-MPC dynamics.³⁷ In such hybrid dynamics, while the solvent molecules interact among themselves through multiparticle collisions, they interact with the solute molecules through solvent-bead intermolecular forces, V_{sb} . The total potential energy of the system is, therefore, given by $V_T = V_{PS} + V_{sb}$ and Newton's equations of motion are used to evolve the system under this potential energy for time

intervals τ between MPC events. This hybrid dynamics also satisfies the conservation laws and correctly describes hydrodynamic interactions among solute species and fluid flows in the solvent.

1. Penetrating solvent model

Hydrodynamic interactions and solvent dissipation can also be included in a heuristic way by dropping the direct interactions between solvent and solute molecules and instead including the solute beads into the MPC step of the dynamics.³⁸ In this scheme, the solvent particles evolve freely between collision steps while the coordinates and momenta of the enzyme and substrate are evolved through Newton's equations of motion under the V_{PS} potential function.

More specifically, to allow for interaction between the solvent and beads, the collision rule is modified to include the velocity of the beads in the local center-of-mass velocity of particles in a cell. The center-of-mass velocity is computed for a cell c containing N_c solvent particles of equal mass m and a single bead of mass M and velocity V via,

$$\mathbf{v}_c = \frac{M}{M_T} \mathbf{V} + \frac{N_c m}{M_T} \sum_{i=1}^{n_c} \mathbf{v}_i, \quad (3)$$

where $M_T = N_c m + M$ is the total mass of particles in the cell and \mathbf{v}_i is the velocity of solvent particle i in cell c . The collision rule for the penetrating solvent model with hydrodynamics is defined as

$$\begin{aligned} \mathbf{V}' &= \mathbf{v}_c + \boldsymbol{\omega} \cdot (\mathbf{V} - \mathbf{v}_c), \\ \mathbf{v}_i' &= \mathbf{v}_c + \boldsymbol{\omega} \cdot (\mathbf{v}_i - \mathbf{v}_c), \end{aligned} \quad (4)$$

for the bead velocity \mathbf{V} and the solvent velocities \mathbf{v}_i . Since the magnitude and direction are conserved in the rotation, particle number, linear momentum, and energy are globally conserved, resulting in proper hydrodynamic flow.

2. Penetrating solvent without hydrodynamics

For the purpose of assessing the importance of hydrodynamic interactions, it is useful to construct an alternative model in which the hydrodynamic effects are not present.^{35,39-41} The collision rule for the penetrating solvent model can be modified by defining the center-of-mass velocity of particles in a cell to be

$$\mathbf{v}_c = \frac{M}{M_T} \mathbf{V} + \frac{N_s m}{M_T} \mathbf{v}_s, \quad (5)$$

where N_s is drawn from a Poisson distribution with mean value ρV_c , where ρ is the number density of solvent in the system and V_c is the cell volume. The total mass is $M_T = M + N_s m$, and \mathbf{v}_s is an effective solvent velocity drawn from a Maxwell-Boltzmann distribution with mass $N_s m$. Since this velocity is drawn at each collision step, the velocity of the solvent is uncorrelated from one collision step to another. In this model, explicit solvent particle dynamics is replaced by the action of the collision operator. Since the velocity of the fluid is completely decorrelated after a single collision step, any dynamic correlations associated with a small value of the ratio of the mean free path to cell length strictly vanish.

III. ENZYMATIC CYCLE DYNAMICS

Complete enzymatic cycles can be simulated using the mesoscopic dynamical scheme described in Sec. II. When the protein, substrates, and solvent molecules are modeled as structureless particles, full MD-MPC dynamics has been used to study the effects of diffusion on enzyme kinetics.⁴² However, in the conditions that pertain to the interior of a cell, even this multi-scale method will not be computationally efficient if both the internal dynamics of the enzymes and the diffusive motion are considered. Under physiological conditions the concentrations of both substrates in the cytoplasm are relatively small^{43,44} (0.14 mM for ADP and 0.001 mM for bPG), while the enzyme concentration is roughly 0.1 mM. If the substrates and enzyme are uniformly distributed in the volume, the radius of the spherical volume around the enzyme containing a single substrate molecule is roughly $r_{\text{ADP}} = 142 \text{ \AA}$ for ADP and $r_{\text{bPG}} = 734 \text{ \AA}$ for bPG. The sphere containing a single enzyme has a radius of $r_{\text{PGK}} = 158 \text{ \AA}$.

Substrate molecules diffuse into the vicinity of an enzyme where binding takes place. The characteristic times for such diffusive dynamics can be estimated from the Stokes-Einstein relation or taken from experimental measurements of the diffusion coefficients of substrates in the cytoplasm. For example, estimating the viscosity of the cytoplasm to be roughly 5 times that of water, namely, $\eta = 0.005 \text{ Kg/(ms)}$, and assuming the substrates have an effective radius $R_S \approx 5 \text{ \AA}$, the Stokes-Einstein law $D = k_B T / (6\pi \eta R_S)$ gives a value of $D = 10^{-10} \text{ m}^2/\text{s}$, a value that is within the experimental range of measured D values. Given these conditions, we shall see that the ADP substrate binds typically before $5 \mu\text{s}$, whereas the binding time of the bPG is very broadly distributed over many decades and is the main factor determining the reaction time. For this reason, we suppose that ADP is bound to the enzyme and focus on the binding of bPG.

From these considerations it is evident that the enzymatic dynamics has a significant diffusion-influenced component; therefore, it is computationally inefficient to follow individual trajectories of the diffusive dynamics of substrates and enzymes in the solvent for the long times needed for enzyme-substrate encounters. Consequently, it is useful to decompose the process into portions, where the substrates diffuse in the solvent without directly interacting with proteins, and portions where these species interact through direct intermolecular forces. The diffusive portions of the dynamics can be treated to a good approximation by analytical methods, while in the interacting portions the mesoscopic dynamical scheme can be used to describe details of the binding, conformational changes, and reaction. These considerations suggest a stochastic model for the cycle dynamics that combines these types of dynamical evolution.

A. Stochastic model for enzyme dynamics

Initially, suppose the bPG substrate moves diffusively in a volume with radius r_{bPG} surrounding the enzyme without any influence on its motion due to the presence of an enzyme. Since the concentration of enzyme is a factor of 100 times that of the bPG, the number of enzymes in this volume should be Poisson distributed with an average number of 100 enzymes

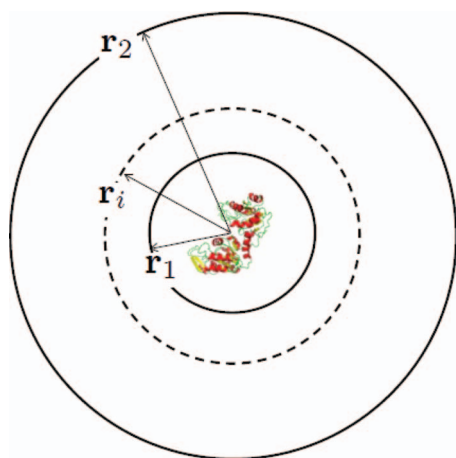


FIG. 3. Structure of the model used in the simulation of the diffusive encounters of the substrate with the enzyme and the full dynamics in the enzyme vicinity. The outer circle denotes the spherical volume with radius r_2 containing a single enzyme molecule, while the inner-most circle with radius r_1 denotes the spherical volume around the enzyme within which a full dynamical calculation is carried out. Within r_1 the dynamical evolution is followed until the substrate leaves the spherical volume with radius $r_i > r_1$ or binds and reacts.

in the volume if there is no correlation in the density of enzymes. We assume the binding of the bPG to any enzyme in the volume occurs in the following way: At any given time, the bPG is within the spherical volume with radius $r_2 = r_{\text{PGK}}$ of some enzyme, which is chosen to be equal to the volume around the enzyme that contains a single substrate molecule (see Fig. 3). The substrate can either diffuse to the binding region of this enzyme, or out of its volume. The binding probability is dependent on how far the substrate is from the enzyme, here, taken to be r_1 . If the substrate diffuses out of the volume of the enzyme, the first passage time out of the spherical volume can be recorded. Subsequently, the position of the bPG relative to another enzyme is assumed to be randomly distributed in the volume of this other enzyme, and the process is repeated until the substrate passes through the inner spherical volume of radius r_1 around an enzyme.

The point where the substrate passes through the inner sphere is uniformly distributed on the surface of the sphere. After passing through the inner sphere, the substrate will either bind to the enzyme or move out of the inner sphere and pass through a sphere of intermediate size (with radius r_i with $r_1 \leq r_i \ll r_2$). Since the dynamics of the substrate is influenced by the presence of the enzyme and the solvent flow around it, the dynamics is no longer diffusive and must be simulated explicitly as described in Sec. II. Starting from a uniformly chosen point on the surface of the sphere with radius r_1 , if the substrate does not bind to the active site, the particle continues to diffuse starting from a radial distance of r_i and either will be reabsorbed by the inner sphere or pass out of the volume through the outer sphere.

For most of the dynamical evolution, the substrate diffuses freely without explicit solvent flow effects or influence from the enzyme. For this type of dynamics, analytical solutions to the diffusion equation can be used. The final regime to be described consists of the dynamics of the substrate from the surface of the inner sphere with radius r_1 to the active site

on the enzyme in the presence of solvent. This final regime should be simulated directly, since the hydrodynamic motion of the solvent influences both substrate and enzyme motion.

More specifically, the algorithm can be stated as follows:

- (1) At the initial time if the substrate is at r_2 a position \mathbf{r} , $r_1 < r < r_2$, is randomly selected.
- (2) Given a uniformly distributed random number $\xi_r \in [0, 1]$, if $\xi_r \leq P_1(r)$ the substrate is absorbed at the r_1 boundary, otherwise it is absorbed by the r_2 boundary. Here, $P_1(r)$ is the probability that the substrate is absorbed at the r_1 boundary in the infinite time limit.
- (3) If it is absorbed at r_2 , a time is drawn from $P_2(t|r)$, the first-passage time density for absorption onto a sphere with radius r_2 starting a distance r from center, and used to update the cycle time.
- (4) If it is absorbed at r_1 , a time is drawn from $P_1(t|r)$, the first-passage time density for absorption onto a sphere with radius r_1 starting a distance r from center, and used to update the cycle time. Starting at r_1 , a full mesoscopic dynamical simulation is then carried out until reaction occurs or the substrate reaches the r_i boundary. If the dynamics results in a reaction, the time for the reaction to proceed and the products to diffuse away from the active site is added to the cycle time and the enzymatic cycle is complete. If instead the substrate reaches r_i without reaction, this time is added to the cycle and we return to step (2) to continue the dynamics until the cycle is complete. The boundary at r_i is chosen to be significantly larger than r_1 to minimize the blocking effect of the enzyme leading to a non-uniform distribution of points of absorption on the absorbing sphere. The explicit forms of the $P_{1,2}(r)$ and $P_{1,2}(t|r)$ probabilities are given in Appendix B.

1. Fully stochastic model

An alternative way of accounting for the effects of the full mesoscopic evolution is to pre-compute the probability distributions of times for completion of the reaction, $P_r(t)$, and binding failure, $P_f(t)$. To compute these probabilities, an ensemble of trajectories that start at a uniformly chosen position on the inner sphere at radius r_1 is evolved until either the substrate binds and reacts or the unbound substrate escapes and passes through an absorbing sphere at intermediate distance r_i from the binding site. The binding probability can be estimated from the fraction of reactive trajectories and the probability densities $P_r(t)$ and $P_f(t)$ can be constructed using analytical fits to the estimated cumulative distribution functions obtained from the reaction and failure times.⁴⁵ Given this information, once the substrate is at r_1 in step (4), the binding probability can be used to determine if reaction will occur and the reaction time can be drawn from $P_r(t)$ and used to complete the cycle, or if no reaction occurs the time can be drawn from $P_f(t)$ and used to increment the time.

IV. SIMULATION OF PGK ENZYME KINETICS

The simulations employing hybrid MD-MPC dynamics were carried out on a system comprising a single PGK

enzyme with bound ADP, a bPG substrate molecule and solvent molecules in a cubic box of length L with periodic boundary conditions. The units used in the simulation are given in terms of length ℓ , mass m , energy ϵ , and time τ . In these units the simulation box had length $L = 40$ and contained 640 000 solvent particles of mass $m = 1$, resulting in a density $\rho = 10$. The mass of the beads comprising the enzyme was taken to be $M = 10$, so that the mass ratio of solvent to beads was set to $\mu = M/m = 10$. The solvent particles interact with all beads through the truncated repulsive potential in Eq. (A4) with an adjustable σ , usually taken to be $\sigma = 1$. Simulation of the enzyme-substrate system consists of numerically integrating Newton's equations of motion for all bead and solvent particles that interact with a time step of $\Delta t = 0.005$ for time intervals $\tau = 1$ between multiparticle collisions. For the implementation of the stochastic portions of the model we have chosen $r_2 = 31.6$, $r_i = 9$, and $r_1 = 7$ in simulation cell length units. A cell length is roughly $\ell = 5 \text{ \AA}$ so that $r_{\text{PGK}} = 158 \text{ \AA}$ corresponds to the r_2 value given above in simulation units. The values for r_1 and r_i were chosen to minimize the amount of numerical simulation required while allowing for good statistics for various numerically computed densities. Information from such direct simulations of the dynamics is required for both the diffusive encounters between the enzyme and substrate and the subsequent binding and reaction processes. These two aspects are discussed in Subsections IV A–IV C.

A. Diffusive dynamics

Although the diffusive encounters between the substrate and enzyme are treated analytically, these calculations require the diffusion coefficient D of the substrate as input into the analytical formulas for the first passage time probabilities. Therefore, in this subsection we present results for D for the explicit interaction and penetrating solvent models. Since the substrate does not interact with the enzyme in this regime we need only consider the motion of the substrate in pure solvent.

1. Explicit interaction model

In the explicit interaction model the substrate interacts with the solvent molecules through repulsive Lennard-Jones (LJ) potentials and the solvent molecules undergo multiparticle collisions. The diffusion coefficient may be determined directly by simulation from the velocity autocorrelation function or the mean square displacement. Hydrodynamic effects are included in the MD-MPC dynamics and these give rise to long time tails in the velocity correlation function which make important contributions to the diffusion coefficient. For this reason it is convenient to estimate D by extrapolation of the time-dependent diffusion coefficient to infinite time since

$$D(t) = \frac{1}{3} \int_0^t dt \langle \mathbf{V}(t) \cdot \mathbf{V} \rangle \sim D - \frac{\alpha_D}{\sqrt{t}}, \quad (6)$$

where $\alpha_D = (2/3)(4\pi(\eta + D))^{-3/2}(m\rho)^{1/2}$ with η the shear viscosity. The power-law behavior of this quantity arises from coupling of the substrate to hydrodynamic modes of the solvent. The time-dependent diffusion coefficient is plotted

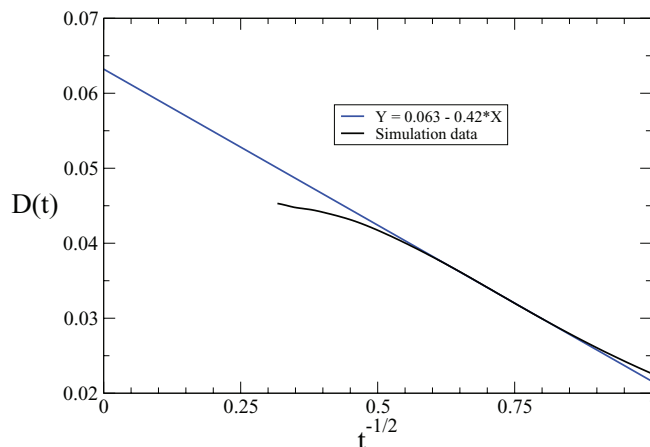


FIG. 4. The simulated value of the diffusion coefficient compared to the estimated time-dependent diffusion coefficient, $D(t)$, in Eq. (6), versus $t^{-1/2}$ for an isolated Brownian particle with mass ratio = 10, $\rho = 10$, $k_B T = 1/3$, $\sigma = 0.5$. From the fit of the data, the value of the diffusion coefficient is $D = 0.063$ in units of ℓ^2/τ .

versus $t^{-1/2}$ in Fig. 4 and shows the long-time power-law behavior. For a substrate with mass $M = 10$ in a solvent with $\rho = 10$, $k_B T = 1/3$, substrate-solvent Lennard-Jones parameters $\sigma = 0.5$ and $\epsilon = 1$, we find $D = 0.063$ in units of ℓ^2/τ . Hydrodynamic effects dominate the contributions to the diffusion coefficient and it is only weakly dependent on the mass of the substrate and solvent molecules. For a very large substrate molecule the diffusion coefficient takes a Stokes-Einstein form and is independent of the mass.

2. Penetrating solvent model

The diffusion coefficient can be computed analytically for the penetrating solvent model. In the collision step, the rotation matrix is uniformly selected from a set of matrices in which the rotation by the angles α and $-\alpha$ around a given set of axes are equally probable. The operation of the rotation matrix on a general vector \mathbf{r} for a rotation by angle α around a unit vector $\hat{\mathbf{n}}$ can be written succinctly as

$$\boldsymbol{\omega} \cdot \mathbf{r} = \mathbf{r} \cos \alpha + \hat{\mathbf{n}}(\hat{\mathbf{n}} \cdot \mathbf{r})(1 - \cos \alpha) + (\mathbf{r} \times \hat{\mathbf{n}}) \sin \alpha. \quad (7)$$

Since the substrate bead behaves as a point particle with respect to hydrodynamic flow, the only contribution to the self-diffusion coefficient comes from the rotation collision step. Hence for this system, the decay of the velocity autocorrelation function for an isolated bead is expected to be a single exponential.

The self-diffusion coefficient for this model can be computed from the velocity autocorrelation function using the trapezoidal rule,

$$D = \frac{1}{3} \int_0^\infty dt \langle \mathbf{V} \cdot \mathbf{V}(t) \rangle \quad (8)$$

$$= \frac{\tau}{3} \left(\frac{1}{2} \langle \mathbf{V} \cdot \mathbf{V} \rangle + \sum_{n=1}^{\infty} \langle \mathbf{V} \cdot \mathbf{V}(n\tau) \rangle \right), \quad (9)$$

where τ is the collision time and the brackets $\langle \dots \rangle$ correspond to an average over the stochastic realizations (choice of

rotation matrices) and the equilibrium distribution of the system. If the matrices are chosen uniformly and the rotation angles α and $-\alpha$ are equally probable, then the Markovian dynamics for a given cell has the limit distribution,

$$P(n, \mathbf{r}_n, \mathbf{v}_n; R, V) = \frac{e^{-\rho}}{V_c^n} \frac{\rho^n}{n!} \Pi_m(\mathbf{v}_n) \times \frac{1}{V_c} \Pi_m(V), \quad (10)$$

where n is the number of solvent particles in the cell containing the tagged particle, V_c is the volume of the cell (here taken to be unity), and $\Pi_m(\mathbf{v}_n)$ is the normalized Maxwell-Boltzmann distribution for a system of n -particles at temperature T . Using this form, one finds that $\langle \mathbf{V} \cdot \mathbf{V} \rangle = 3k_B T/M$, and

$$\begin{aligned} \langle \mathbf{V} \cdot \mathbf{V}(\tau) \rangle &= \frac{1}{n_R} \sum_{i=1}^{n_R} \langle \mathbf{V} \cdot (\mathbf{v}_c + \boldsymbol{\omega}_i \cdot (\mathbf{V} - \mathbf{v}_c)) \rangle \\ &= \langle \mathbf{V} \cdot \mathbf{v}_c \rangle + \langle \mathbf{V} \cdot \bar{\boldsymbol{\omega}} \cdot (\mathbf{V} - \mathbf{v}_c) \rangle, \end{aligned} \quad (11)$$

where $\bar{\boldsymbol{\omega}} = \sum_{i=1}^{n_R} \boldsymbol{\omega}_i / n_R$ and n_R is the total number of rotation matrices. Inserting the stationary density in Eq. (10), and defining the mass ratio $\mu = M/m$, one gets

$$\begin{aligned} \langle \mathbf{V} \cdot \mathbf{V}(\tau) \rangle &= \frac{3k_B T}{M} e^{-\rho} \sum_{n=1}^{\infty} \frac{\rho^n}{n!} \left(1 + (c_\gamma - 1) \frac{n}{n + \mu} \right) \\ &= \frac{3k_B T}{M} \left(1 + \frac{(c_\gamma - 1)\rho}{1 + \mu} M(1, 2 + \mu, -\rho) \right) \\ &\equiv \frac{3k_B T}{M} (1 - \gamma), \end{aligned} \quad (12)$$

where $M(1, 2 + \mu, -\rho)$ is Kummer's function of the first kind⁴⁶ and $c_\gamma = \text{Tr} \bar{\boldsymbol{\omega}}/3$. If there is no correlation between solvent particles occupying the cell containing tagged particles following the collision steps, so that $\langle \mathbf{V} \cdot \mathbf{V}(n\tau) \rangle = (1 - \gamma) \langle \mathbf{V} \cdot \mathbf{V}((n-1)\tau) \rangle$, we conclude

$$D = \frac{k_B T \tau}{M} \left(\frac{1}{2} + \sum_{n=1}^{\infty} (1 - \gamma)^n \right) = \frac{k_B T \tau}{M} \left(\frac{2 - \gamma}{2\gamma} \right), \quad (13)$$

where

$$\gamma = \frac{1 - c_\gamma}{1 + \mu} \rho M(1, 2 + \mu, -\rho). \quad (14)$$

The analytical results for the self-diffusion coefficient are plotted in Fig. 5 as a function of the mass ratio μ for the simulation values $k_B T = 1/3$, $\rho = 10$, and $c_\gamma = 1/3$.

While the diffusion coefficient depends weakly on the mass ratio for the explicit solvent interaction model, it does depend strongly on the mass ratio for the penetrating solvent model. In order to facilitate comparisons between these two solvent interaction models, we choose the mass ratio so that the self-diffusion coefficient of an isolated bead matches that in the interacting solvent model. Note that for the mass ratio $\mu = 10$ used in the interacting solvent model, the self-diffusion coefficient in the penetrating solvent model is substantially larger than in the interacting model ($D = 0.086 > 0.063$), and a mass ratio of roughly $\mu = 28.5$ must be used for the dynamics of the tagged particle to be comparable. The analytical result in Eq. (13) which was used to determine the appropriate mass ratio was obtained by making a molecular

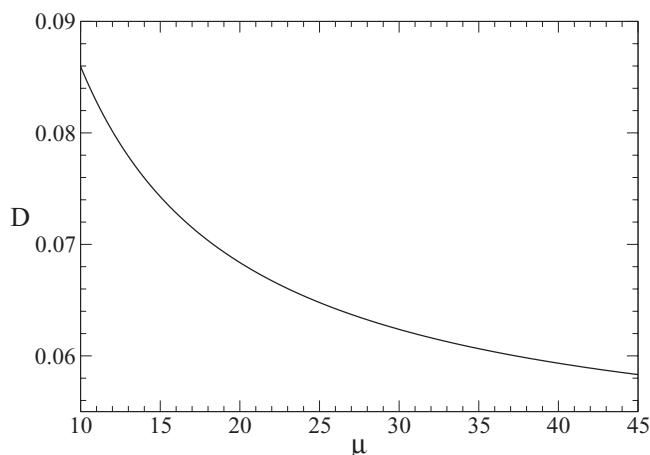


FIG. 5. Plot of Eq. (13) for the self-diffusion coefficient D for a tagged particle in the penetrating solvent model as a function of the mass ratio μ . From this figure we see that if the mass ratio is selected to be $\mu \approx 28.5$ the value of the diffusion coefficient in the penetrating solvent model, $D \approx 0.063$, matches that in the explicit interaction model.

chaos approximation.⁴⁷ To confirm that the correct mass ratio was determined, D was computed directly from simulation with $\mu = 28.5$ and agreement within statistical uncertainties was observed. Finally, we note that the penetrating solvent model without hydrodynamic interactions is exactly given by Eq. (13) since there is no correlation between solvent particles between collisions.

B. Substrate binding and reaction

The position of the bPG substrate was randomly chosen on a spherical shell at a distance $r_1 = 7$ from the active binding site of the enzyme. The distance was chosen so that the bPG substrate does not interact with the active site or other parts of the enzyme. For each realization of the dynamics, the enzyme configuration was equilibrated in the presence of the solvent while constraining the bPG substrate in position. The run was then initiated by randomly drawing the bPG velocity from a Maxwell-Boltzmann distribution at an effective temperature of $k_B T = 1/3$ and releasing the constraint. If the substrate bound to the enzyme (when the substrate reaches its equilibrium distance from the binding site), the time of binding of the bPG was recorded. If instead the distance of the substrate to the active site reached a large value, here taken to be at a substrate-active site distance of $r_i = 9$, the evolution of a realization was terminated and the failure time was recorded. Upon binding, the form of the network potential for the enzyme allows the enzyme to close to an activated form. The time of closing, again determined by a distance criterion between conserved, rigid sections of the enzyme, was recorded. Once the enzyme closed, a reaction time τ_r was drawn from a Poisson distribution (here taken to have a mean reaction time of $\bar{\tau}_r = 25$ time units), which defines the rate at which an unbinding potential was activated by the control parameter ξ .

The probability densities for the time of substrate binding, the closing time of the enzyme after binding, and the overall cycle time are shown in Fig. 6. The analytical fit to

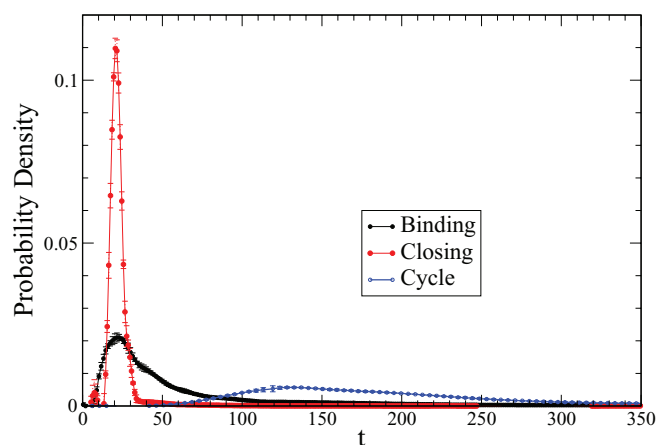


FIG. 6. Probability densities for the time of substrate binding (black), closing time of the protein (red), and the overall cycle time (blue). These probability densities were constructed from analytical fits to the simulation data for the full solvent model as a function of time. The results are for simulation conditions $\mu = 10$, $k_B T = 1/3$, $\rho = 10$, with a solvent-bead interaction $\sigma = 0.5 \ell$, corresponding to $\sigma = 2.5$. Points on the curves are chosen to indicate statistical uncertainties in the construction of the densities.

the densities with bootstrap estimates for uncertainties were computed from the raw data using the procedure described in Ref. 48. A prominent feature in the probability density of binding times is the long algebraic tail, which is a signature of the substrate initially moving away from the enzyme but eventually diffusing into the active site. The form of the tail in this density is consistent with the asymptotic long time behavior for a particle diffusing into an absorbing region in three dimensions. Note that the probability density for the overall cycle time can be decomposed into a convolution of the density for binding, closing, and diffusion away from the binding site after the reaction is complete. Since diffusive motion leads to densities with heavy tails, the overall cycle time density is broad, which is characteristic of algebraic tails.

Another important qualitative feature of the solvent-enzyme model is the variable degree of solvation of the bPG substrate during the binding process. When the distance $\sigma = 0.5$ characterizing the solvent-bead repulsion is large enough, the solvent is unable to penetrate the volume occupied by the enzyme. The bPG substrate binds to a region inside the enzyme that is exposed when the enzyme is in an open conformation. Upon binding, the enzyme closes via a hinge-like mechanism and brings the ADP-bPG substrates near one another enabling the transfer of the phosphoryl group. Less solvent is able to penetrate into the binding pocket of the bPG substrate in the closed conformation of the enzyme, and hence solvent is expelled from the pocket as bPG binds and the enzyme closes, providing a favorable environment for the catalysis.^{10,23}

The expulsion of solvent can be tracked by computing the local solvent density around the bPG substrate as it binds and reacts, as can be seen in Fig. 7. This drying effect is highly sensitive to the choice of the repulsive interaction parameter σ . When $\sigma = 0.5$ (see top panel of Fig. 7), the bound substrate typically has 2 fewer solvent particles solvating it, whereas away from the enzyme the average number of solvating fluid particles corresponds to the value of the bulk density

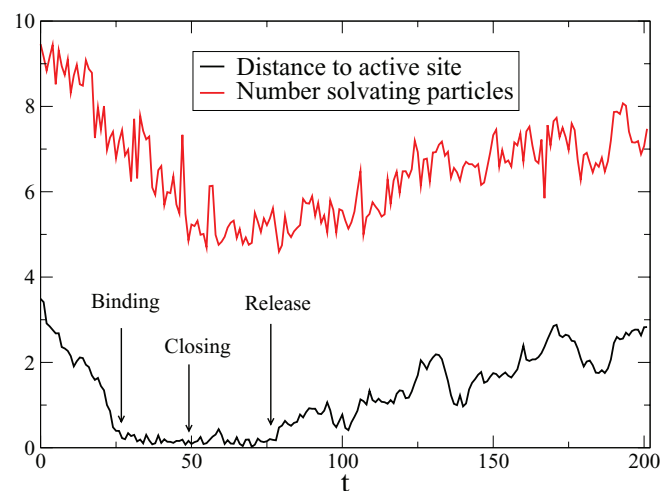
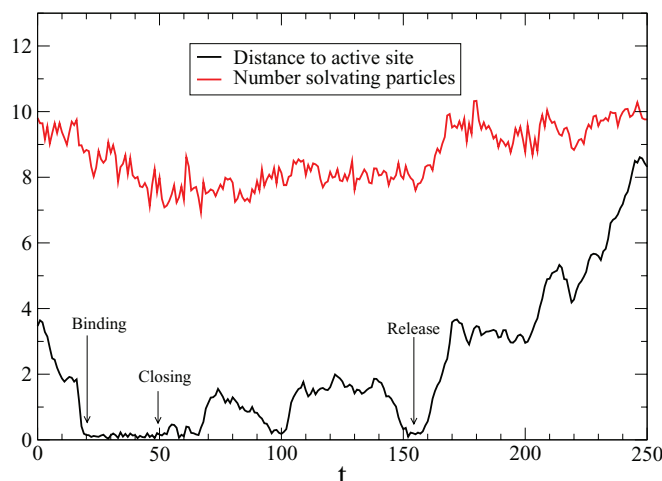


FIG. 7. Time series showing the reduction in the number of solvent particles in the vicinity of the bPG substrate as it binds to the enzyme. The red curves show the number of solvent particles in the cell containing the bPG substrate as a function of time, while the black curves denote the distance of the substrate to the enzyme binding site. (Top) $\sigma = 0.5$, (bottom) $\sigma = 0.7$.

($\rho = 10$). This difference between bulk and bound solvation levels increases as the repulsion parameter σ increases (see bottom panel of Fig. 7, where $\sigma = 0.7$). There are important differences in the qualitative nature of the dynamics when the repulsion parameter becomes large. Although the exterior of the enzyme experiences a larger overall friction, the dissipating effect of the solvent on the enzyme-substrate interaction is decreased in the pocket of the enzyme where the binding occurs. The bPG substrate retains a high kinetic energy upon entering the pocket for a longer period of time due to a limitation in the simple model of the binding process in which the substrate effectively interacts with only a few beads of the enzyme. Because of the limited coupling of the beads in the active site to other beads in the protein, the excess energy of the substrate is slowly dispersed into internal motions of the protein and solvent. For this reason, we focus primarily on a regime in which the solvent rapidly dissipates energy ($\sigma = 0.5$).

In Fig. 8 the probability densities for the binding time, enzyme closing time, and overall cycle time, defined to be the time required for the substrate to diffuse in from distance

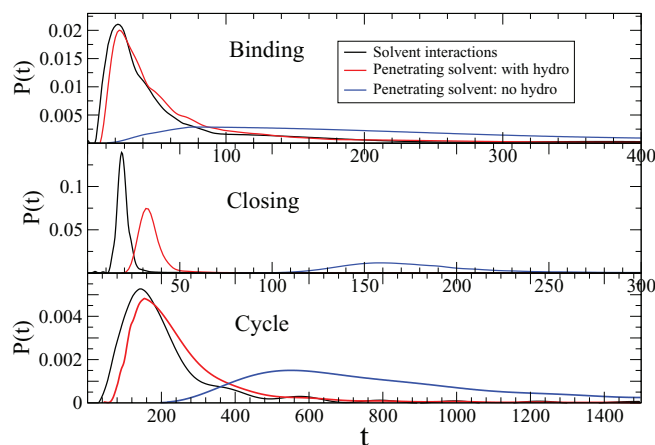


FIG. 8. Probability densities $P(t)$ for the time of substrate binding (top panel), enzyme closing time (middle panel), and total reaction cycle time (bottom panel). The black curves correspond to results for the interacting solvent model, the red curves correspond to the results for the penetrating solvent model with hydrodynamics, and the blue curves are the results for the penetrating solvent model without hydrodynamics.

r_1 , react and the products to diffuse out to distance r_i , are presented. Looking at the top panel, we see that the probability densities of the binding time for the interacting and penetrating solvent models are comparable once the dynamics has been properly scaled by the mass ratio. This similarity is not surprising, as the time scale for binding is primarily determined by diffusive motion and is not sensitive to the level of solvation of the substrate by the fluid particles. However, the absence of hydrodynamic flow around the enzyme and substrate has a profound effect on both the form of the probability density, which is significantly broadened, and the mean binding time, which is shifted by a factor of roughly a factor of three. In addition, the binding probability is significantly reduced from $P_r = 0.078$, in the presence of hydrodynamics, to $P_r = 0.03$, which can have a significant impact on the density for the overall substrate conversion time when the concentration of substrates is elevated. Note that the probability density of binding times has a strong tail for all models, indicative of the importance of the diffusive dynamics experienced by the substrate.

The time required for the enzyme to close after binding is noticeably different in all three models. The penetrating solvent model does not account for solvent expulsion as the enzyme closes, and therefore has a higher net friction and longer time scale than is present in the explicit interaction model. Once again, the effect of hydrodynamics is significant, and shortens the time required for the enzyme to close.

The overall cycle time density is a convolution of the binding time and closing time densities, and is therefore different for all three models.

C. Fully stochastic model

A stochastic procedure can be implemented for the overall enzymatic process using data from the numerical simulations and the computed values of the binding probability starting from a radial distance of r_1 . If the binding is accepted

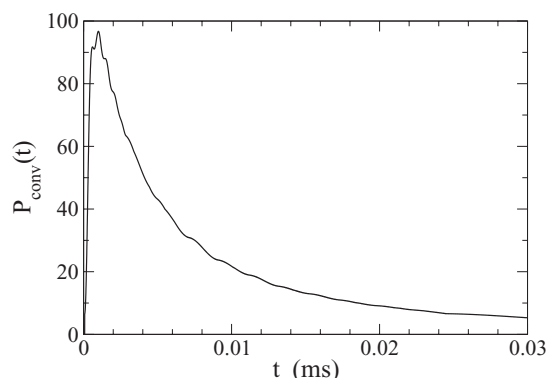


FIG. 9. Probability density $P_{\text{conv}}(t)$ of the substrate conversion time to products versus time expressed in milliseconds for the explicit solvent model. The other models yield essentially identical results since the substrate conversion is determined primarily by diffusion when the substrate is at physiological concentrations.

starting from the inner sphere with probability P_r , which for the explicit solvent model is approximately $P_r = 0.078$, the overall cycle time for the reactive process can be added to the overall time for the process by drawing from the numerically-obtained probability densities and cumulative distributions. To carry out the procedure, the reaction time is drawn by numerically solving the equation $C_{\text{cycle}}(t_u) = u$ for the time t_u using bisection or Newton-Raphson methods, where u is a random variable drawn uniformly from the unit interval. Here, $C_{\text{cycle}}(t)$ is the cumulative distribution for the cycle obtained from the simulation.

To convert the system collision time into physical units, note that the self-diffusion coefficient in system units is $0.06 \ell^2/\tau$. Equating this with the desired value of the diffusion coefficient in the cytoplasm of roughly $D = 1 \times 10^{-10} \text{ m}^2/\text{s}$, we conclude that $\tau = 1.5 \times 10^{-10} \text{ s}$. Using this scaling, we find that the typical time required for the PGK enzyme to close following binding of both substrates is on the order of 3 to 6 ns for the solvent models incorporating hydrodynamic flow, which is consistent with experimental^{23,49} and simulation²² studies of the enzyme domain motions.

The probability density $P_{\text{conv}}(t)$ of substrate conversion times is shown in Fig. 9.

Somewhat surprisingly, no difference in the probability density of substrate conversion time is readily observable at the enzyme concentration studies here even though the binding probability is more than two times larger in the presence of hydrodynamics than in its absence. This is due to the multiple convolutions of the first passage time densities which have heavy and prominent tails that tend to smooth out observable differences after multiple convolutions.

V. SUMMARY

A stochastic method for computing the probability density of the time required for the enzymatic catalysis of a substrate to product was constructed. The method consists of combining analytical computations of binding probabilities and first-passage times of a substrate diffusing between two concentric absorbing spheres with explicit simulation of

motion of the substrate in the immediate vicinity of the enzyme. Once the explicit simulations have been performed and the data analyzed in terms of binding probabilities and first passage time densities, the method allows the probability density of the time required for the phosphate transfer to be computed at a variety of enzyme concentrations.

The method was illustrated by considering the catalytic transfer of a phosphate group from bPG to a bound ADP substrate by the phosphoglycerate kinase enzyme under physiological conditions. The binding probability and phosphoryl group transfer times for a substrate diffusing in a 0.1 mM concentration of phosphoglycerate kinase were computed under three different solvent conditions using a network model of the enzymatic system constructed from the morphing analysis of the conformational change between the open and closed conformations^{28,29} of the enzyme. The solvent models were chosen to selectively account for various degrees of correlated solvent motion to probe the importance of collective flow effects on the enzyme dynamics. It was demonstrated that dynamical solvent flow effects assist the binding of the substrate to the active site of the enzyme and facilitate the hinge motion of the enzyme that leads to its closing. Two different models that incorporate hydrodynamic flow effects, one with direct solute-solvent interactions and another penetrating solvent model where solvent particles are treated as point particles in their interactions with the substrate and protein, have similar binding probabilities and cycle time densities. However, the density profiles of the solvent near the active site as the enzyme closes post-substrate binding differ, since expulsion of the solvent from the binding pocket is not possible for the penetrating-solvent model. In contrast, a Smoluchowski-type model in which all beads feel a friction that is independent of the conformation of the enzyme is characterized by a lower substrate binding probability and a shift in the cycle time density to larger time scales relative to the models incorporating hydrodynamic effects. The lower substrate binding probability leads to a detectable shift in the maximum appearing in the density of substrate conversion times.

The validity of the stochastic method presented here relies on a number of assumptions that are questionable for the behavior of the enzymatic system in a cellular environment. It has been assumed that the enzymes are homogeneously distributed with no correlation between their positions in the volume. It is quite possible that the enzymes are, in fact, locally clustered in the cytoplasm in a way that effectively reduces the distance between them and the substrates thereby enhancing their efficiency. This is likely to be the case if there is correlation between the spatial location of the phosphoglycerate kinase enzyme and enzymes, such as, glyceraldehyde phosphate dehydrogenase that act earlier in glycolysis. In addition, it has been assumed that the dynamics of the substrate in the complex, crowded cytoplasm is diffusive, which may be reasonable on long time scales but less accurate on the time scale of solvent motion. However, subdiffusive motion of proteins and finite-size probe molecules has been seen in crowded cellular environments.⁵⁰⁻⁵³ Nonetheless, assuming substrates do move diffusively in the cytoplasm at long times, the diffusive nature of the substrate dynamics leads to a broad distribution

of substrate conversion times that differs substantially for the exponential distribution one might anticipate from mass action kinetics.

It is straightforward, though computationally intensive, to incorporate more detailed models of the enzymatic system to produce quantitatively accurate results. This is readily accomplished by performing all atom simulations of the system complete with detailed molecular mechanical-based interaction potentials and quantum-mechanical analysis of chemical reaction pathways. Nonetheless, it is likely that the observation that the solvent flow assists the binding and subsequent protein motions will also be observed in more detailed models of the enzymatic system.

ACKNOWLEDGMENTS

Computations were performed on the GPC supercomputer at the SciNet HPC Consortium, which is funded by the Canada Foundation for Innovation under the auspices of Compute Canada, the Government of Ontario, the Ontario Research Fund Research Excellence and the University of Toronto.

This work was supported in part by grants from the Natural Sciences and Engineering Council of Canada. The authors would like to Dr. Ramses van Zon for useful discussions.

APPENDIX A: PGK POTENTIAL FUNCTIONS

In this Appendix we give the detailed form of the potential function V_{PS} that governs the dynamics of the protein and its interactions with the bPG substrate.

Bonds in the set \mathcal{B}_c of common links were assigned bond potentials $V_c(r_{ij})$ constructed in the following way. The potentials for the common links in the open and closed configurations of the enzyme, V_{co} and V_{cc} , are given by

$$V_{co,cc} = \frac{k_h}{2} \sum_{(ij) \in \mathcal{B}_{hc}} (R_{ij} - l_{ij}^{(o,c)})^2 + \epsilon \sum_{(ij) \in \mathcal{B}_{sc}} \left(5 \left(\frac{\sigma_{ij}^{(o,c)}}{R_{ij}} \right)^{12} - 6 \left(\frac{\sigma_{ij}^{(o,c)}}{R_{ij}} \right)^{10} \right), \quad (\text{A1})$$

where the parameters $l_{ij}^{(o,c)}$ and $\sigma_{ij}^{(o,c)}$ were determined by the equilibrium distances for the harmonic and soft-common links in the open and closed conformations and k_h is the force constant for the hard elastic network bonds. Given this input, the potential for the common interactions V_c was taken to be the lowest eigenvalue of a two-dimensional empirical valence bond matrix with constant off-diagonal elements Δ , so that²⁵

$$V_c = \frac{1}{2} ((V_{co} + V_{cc}) - ((V_{co} - V_{cc})^2 + 4\Delta^2)^{1/2}). \quad (\text{A2})$$

This form of the potential allows the system to smoothly switch between stable open and closed configurations. Links in the soft-open, \mathcal{B}_{so} , and soft-closed, \mathcal{B}_{sc} sets were assigned bond potentials

$$V_s(R_{ij}) = \epsilon \left(5 \left(\frac{\sigma}{R_{ij}} \right)^{12} - 6 \left(\frac{\sigma}{R_{ij}} \right)^{10} \right) \quad (\text{A3})$$

with identical forms. In addition, monomeric beads representing amino acid residues repel one another at short distances according to a truncated and scaled LJ potential,

$$V_r = \sum_{\langle ij \rangle} \epsilon_{bb} \left(\left(\frac{\sigma_{bb}}{R_{ij}} \right)^{12} - 2 \left(\frac{\sigma_{bb}}{R_{ij}} \right)^6 + 1 \right) \theta(\sigma_{bb} - R_{ij}), \quad (\text{A4})$$

with minimum at σ_{wbb} , where $\theta(x)$ is the Heaviside function. The bPG substrate, represented by a single bead with coordinate \mathbf{R} , also interacts with all beads in the protein through a repulsive LJ potential of this form, $V_r^{(b)}(R_{bi})$, where $R_{bi} = |\mathbf{R} - \mathbf{R}_i|$ with ϵ_{bs} and σ_{bs} energy and distance parameters.

1. Interactions governing the reactive event and conformational changes

The binding interaction $V_b^{(b)}(\mathbf{R}, \mathbf{R}_0^a, \mathbf{R}_1^a, \mathbf{R}_2^a)$ between the bPG substrate at position \mathbf{R} and the enzyme was designed to depend on the distance between the substrate and bead with coordinate \mathbf{R}_1^a , as well as the orientation of the substrate with respect to a coordinate frame determined by three beads defining the binding pocket of the enzyme. Defining the relative position vector $\mathbf{R}_{S1} = \mathbf{R} - \mathbf{R}_1^a = R_{S1} \hat{\mathbf{R}}$ with magnitude R_{S1} and direction $\hat{\mathbf{R}}$ of the substrate with respect to a coordinate system centered on the binding site \mathbf{R}_1^a , the projection $R_{S1}^z = \hat{\mathbf{R}} \cdot (\hat{\mathbf{R}}_{10}^a \times \hat{\mathbf{R}}_{21}^a)$ is computed, where $\hat{\mathbf{R}}_{ij}^a$ is the unit vector along $\mathbf{R}_{ij}^a = \mathbf{R}_i^a - \mathbf{R}_j^a$. The binding potential is then taken to be

$$V_s^{(b)} = f(R_{S1}) \left[\epsilon \left[\left(\frac{\sigma_{bb}}{R_{S1}} \right)^{12} - \left(\frac{\sigma_{bb}}{R_{S1}} \right)^6 - 3 \left(\frac{\sigma_{bb}}{R_{S1}} \right)^2 \right] + K_S \left(\frac{\sigma_{bb}}{R_{S1}} \right)^{12} (1 - (R_{S1}^z)^2) \right] \theta(-R_{S1}^z), \quad (\text{A5})$$

where $K_S = 1.5$ in the energy units. In Eq. (A5), $f(R)$ is a smooth cut-off function

$$f(R) = \begin{cases} 1, & R < R_\ell \\ \frac{(R_u - R)^2}{(R_u - R_\ell)^3} (R_u - 3R_\ell + 2R), & R_\ell \leq R \leq R_u \\ 0, & R > R_u \end{cases} \quad (\text{A6})$$

where the upper and lower cut-off values are set to $R_u = 3\sigma$ and $R_\ell = 2.5\sigma$. The potential insures that the optimal angle of approach and binding of the substrate in the active site pocket is along the $\hat{\mathbf{R}}_{21}^a \times \hat{\mathbf{R}}_{10}^a$ direction. In principle, the excluded volume interactions of the substrate bead with the enzyme beads are sufficient to determine the binding pathway of the substrate, while the orientational dependence of the binding potential in Eq. (A5) restricts the binding location in the active site.

As the substrate binds it triggers conformational changes in the protein that lead to hinge closing to bring the bPG and ADP substrates into proximity for the phosphoryl group transfer. Thus, as bPG interacts with the protein in the course of binding to the active site, the open protein configuration is destabilized with respect to the closed configurations, driving the enzyme towards the closed conformation. To achieve this conformational change in the network model, the interaction potentials for the soft, non-common set of links are modified.

We define the reaction coordinate ξ , where

$$\xi = \frac{1}{2} (1 + \tanh x), \quad (\text{A7})$$

where

$$x = \frac{(R_{b1} - R_{b1}^o)^2}{(R_{b1} - R_{b1}^c)^2} - \frac{(R_{b1} - R_{b1}^c)^2}{(R_{b1} - R_{b1}^o)^2}, \quad (\text{A8})$$

and R_{b1}^o is the initially large distance between the substrate and the binding site in the open configuration and R_{b1}^c is the same distance in the bound, closed complex. Since the substrate is unbound and hence far from the binding pocket in the starting configuration, $R_{b1}^o \gg R_{b1}^c$. Note that when the substrate is far from the enzyme, x is large and negative and $\xi \approx 0$, whereas x becomes large and positive as the substrate moves towards the binding site with the result that $\xi \approx 1$ upon binding. Given this reaction coordinate, the soft, non-common potential function is taken to be

$$V_{nc} = \xi \sum_{\langle ij \rangle \in B_{sx}} V_s(r_{ij}) + (1 - \xi) \sum_{\langle ij \rangle \in B_{so}} V_s(r_{ij}). \quad (\text{A9})$$

The protein-substrate interaction potential is given by the sum of these contributions,

$$V_{PS}(\mathbf{R}^{N_p}, \mathbf{R}; \xi(R_{S1})) = V_c + V_r + V_r^{(b)} + V_s^{(b)} + V_{nc}. \quad (\text{A10})$$

After binding, the reaction coordinate ξ is treated as an external control parameter that is governed by the equation,

$$\xi(t) = \begin{cases} 1 - t/\tau_r & \text{if } t \leq \tau_r \\ 0 & \text{otherwise,} \end{cases} \quad (\text{A11})$$

where τ is the reaction time drawn from an exponential distribution $P(\tau_r) = \bar{\tau}_r^{-1} e^{-\tau_r/\bar{\tau}_r}$ and $\bar{\tau}_r$ is the average reaction time. Upon completion of the reaction when $\xi = 0$, the interaction between the substrate in the binding pocket and the binding site is changed to a repulsive Lennard-Jones interaction to reflect the unstable interaction of the altered substrate and the binding pocket. Since $\xi = 0$, the closed configuration is unstable and the enzyme reopens, completing the cycle. In this treatment, the reaction is treated irreversibly and the surrounding solvent absorbs energy from the chemical process, leading to a slight heating of the solvent. The average reaction time $\bar{\tau}_r$ is taken to be 25 time units, corresponding to a physical reaction time of roughly 2.5 ns. Note that the precise value for the average reaction time is unimportant for looking at the qualitative effects of the solvent environment on the dynamics of the enzymatic system. Detailed quantum chemical calculations are required to determine if this estimate of the reaction time from the metastable bound state to a final state consisting of the products bound in a closed conformation of the enzyme is reasonable.

APPENDIX B: DIFFUSION OF SUBSTRATE TO A REGION NEAR ENZYME

The first passage time distribution $P(t|\mathbf{r}_0)$ for a Brownian walker starting from position \mathbf{r}_0 at time $t = 0$ onto a sphere

centered at the origin can be computed from the survival probability distribution $F(t|\mathbf{r}_0)$ using

$$P(t|\mathbf{r}_0) = -\left.\frac{dF(t|\mathbf{r}_0)}{dt}\right|_{\text{sphere}}, \quad (\text{B1})$$

where the derivative of $F(t)$ only includes the flux of walkers into the sphere and

$$F(t|\mathbf{r}_0) = \int_{\Omega} d\mathbf{r} P(\mathbf{r}, t; \mathbf{r}_0). \quad (\text{B2})$$

In Eq. (B2), $P(\mathbf{r}, t; \mathbf{r}_0)$ is the conditional probability of finding the walker at position \mathbf{r} at time t given that it was initially at \mathbf{r}_0 , and Ω is the domain of the system. We shall assume that the walker is confined between two absorbing spheres of radii $r_- = r_1$ and $r_+ = r_2$. Given the spherical boundaries of the domain, it is natural to express positions in terms of spherical polar coordinates (r, θ, ϕ) , where the z-axis from which the angle θ is measured relative to the vector connecting the origin to a specific point \mathbf{r}_p on the inner sphere. The angle ϕ can be measured from the plane containing the vectors \mathbf{r}_p and \mathbf{r}_0 so that $\phi_0 = 0$. The evolution of the conditional probability is determined by the diffusion equation

$$\frac{\partial P}{\partial t} = D \nabla_r^2 P, \quad (\text{B3})$$

and satisfies the boundary condition $P(\mathbf{r}, 0; \mathbf{r}_0) = \delta(\mathbf{r} - \mathbf{r}_0)$. From the diffusion equation, we find that the first-passage distribution through a spherical domain at radial distance r_- is given by

$$\begin{aligned} P(t|\mathbf{r}_0) &= -\int_{\Omega} d\mathbf{r} \frac{\partial P}{\partial t} = -D \int_{\Omega} d\mathbf{r} \nabla_r^2 P \\ &= -D \int_{\partial\Omega} dS \hat{\mathbf{r}} \cdot \nabla_r P \\ &= D \int_{\text{sphere at } r_-} dS \frac{\partial P}{\partial r}, \end{aligned} \quad (\text{B4})$$

where the second line follows from Green's theorem. The domain Ω contains all points with radii in the range $[r_-, r_+]$, and the integral over the inner sphere can be written to obtain

$$P(t|\mathbf{r}_0) = Dr_-^2 \int_0^\pi d\theta \sin \theta \int_0^{2\pi} d\phi \frac{\partial P(r_-, \theta, \phi, t; \mathbf{r}_0)}{\partial r}. \quad (\text{B5})$$

The diffusion equation may be solved for arbitrary coordinates \mathbf{r} and \mathbf{r}_0 in the presence of absorbing boundaries by expanding the density $P(\mathbf{r}, t|\mathbf{r}_0)$ in spherical polar coordinates. The absorbing boundary conditions require that

$$\begin{aligned} P(r_-, \theta, \phi, t; r_0, \theta_0, \phi_0) &= 0 \\ P(r_+, \theta, \phi, t; r_0, \theta_0, \phi_0) &= 0. \end{aligned} \quad (\text{B6})$$

Although a general series solution in spherical harmonic functions for $P(\mathbf{r}, t|\mathbf{r}_0)$ is possible, the spherically averaged flux $F(t|\mathbf{r}_0)$ and first-passage time distribution $P(t|\mathbf{r}_0)$ are simple to obtain since only the first, spherically-symmetric term in the expansion remains. From the differential equation for the expansion coefficients, one finds that the Laplace transform $\tilde{P}(s|\mathbf{r}_0) = \int_0^\infty dt e^{-st} P(t|\mathbf{r}_0)$ of the first passage time density

$P(t|\mathbf{r}_0)$ for the inner sphere is given by⁵⁴

$$\begin{aligned} \tilde{P}(s|\mathbf{r}_0) &= \left(\frac{x_-}{x_0}\right)^{1/2} \frac{C_{1/2}(x_0, x_+)}{C_{1/2}(x_-, x_+)} \\ &= \left(\frac{r_-}{r_0}\right)^{1/2} \frac{C_{1/2}(x_0, x_+)}{C_{1/2}(x_-, x_+)}, \end{aligned} \quad (\text{B7})$$

where x_0 is the scaled variable $x_0 = \sqrt{s/D} r_0$, $x_+ = \sqrt{s/D} r_+$, $x_- = \sqrt{s/D} r_-$, and $C_v(a, b) = I_v(a)K_v(b) - I_v(b)K_v(a)$, where $I_v(x)$ and $K_v(x)$ are modified Bessel functions. For a large outer sphere for which $r_+ \gg r_-$, $C_{1/2}(x, x_+) \rightarrow -I_{1/2}(x_+)K_{1/2}(x)$. Considering a particle that can start at any point on a spherical shell at $r = r_0$, we can write $\tilde{P}(s|\mathbf{r}_0) \sim \sqrt{r_-/r_0} K_{1/2}(x_0)/K_{1/2}(x_-)$.

Noting that

$$k_0(x) = \sqrt{\frac{\pi}{2x}} K_{1/2}(x) = \frac{\pi}{2x} e^{-x},$$

the Laplace transform $\tilde{P}_1(s|\mathbf{r}_0)$ of the first passage density to the inner sphere can be approximated by

$$\tilde{P}_1(s|\mathbf{r}_0) = \frac{k_0(x_0)}{k_0(x_-)} = \left(\frac{r_-}{r_0}\right) e^{-\sqrt{s/D}(r_0-r_-)}, \quad (\text{B8})$$

which can be explicitly inverted to obtain the normalized first-passage distribution $P_1(t|r)$ for particles that are absorbed at the inner sphere radial distance r_1 starting from the spherical shell at distance r ,

$$P_1(t|r) = \frac{(r-r_1)}{\sqrt{4\pi Dt^3}} e^{-(r-r_1)^2/(4Dt)}. \quad (\text{B9})$$

This result is plotted in Fig. 10 (top panel). Note that the fraction of particles absorbed at the inner sphere in the infinite time limit can be computed from the $s = 0$ limit of Eq. (B7), yielding

$$\tilde{P}_1(s=0|r) = P_1(r) = \frac{r_1}{r} \frac{r_2 - r}{r_2 - r_1}.$$

The fraction of particles absorbing at the outer boundary in the infinite time limit is $P_2(r) = 1 - P_1(r)$. These probabilities play an important role in the stochastic simulation algorithm.

The first-passage time density at the outer sphere is obtained similarly, although the inversion of the Laplace transform $\tilde{P}_2(s|r)$ is complicated since

$$\begin{aligned} \tilde{P}_2(s|r) &= \left(\frac{r_2}{r}\right)^{1/2} \frac{C_{1/2}(x, x_2)}{C_{1/2}(x_1, x_2)} \\ &= \frac{r_2}{r} \frac{\sinh x_1 e^{-x} - \sinh x e^{-x_1}}{\sinh x_1 e^{-x_2} - \sinh x_2 e^{-x_1}}, \end{aligned}$$

where $x = \sqrt{s/D} r$ and $x_i = \sqrt{s/D} r_i$. Although the density can be approximated using series expansions for Θ -functions, it is a simple matter to invert $\tilde{P}_2(s|r)$ numerically using the Stehfest algorithm.^{55,56}

To draw a random time from the first-passage density $P_1(t|r)$, one first defines the cumulative distribution $C_1(t|r) = \int_0^t d\tau P_1(\tau|r) = 1 - \text{erf}((r-r_1)/\sqrt{4Dt})$. Suppose u is drawn uniformly from the unit interval. Setting $u = C_1(t_u|r)$

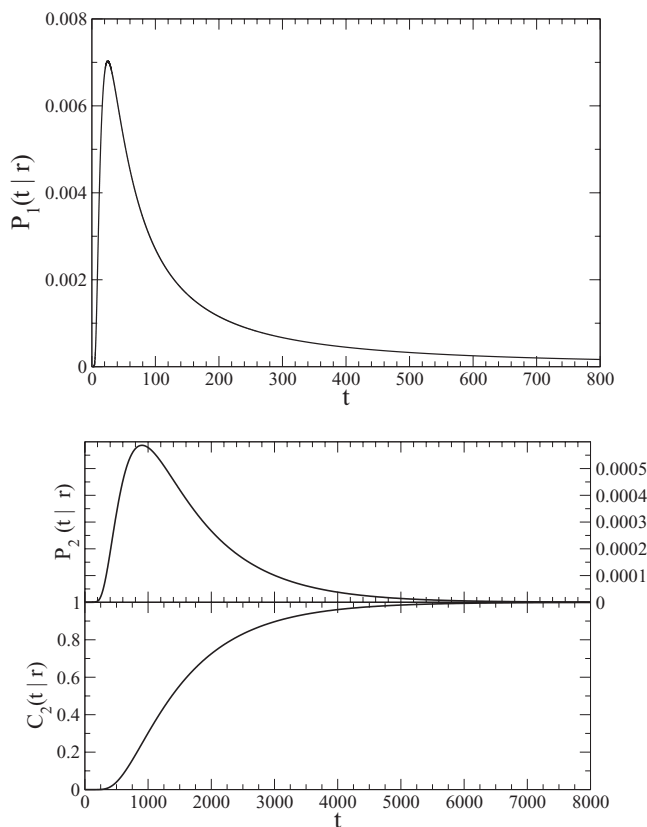


FIG. 10. Absorption time probability density versus time. The top panel is the absorption time for the absorption onto an inner sphere at $r_1 = 7$ starting from a radial distance $r = 10$ in length units ℓ . The bottom panel shows the absorption time density (top) and cumulative distribution (bottom) for the outer sphere, where the outer absorbing sphere radius is set to be $r_2 = 31.6$ and $r = 10$.

and solving for t_u gives

$$t_u = \frac{(r - r_1)^2}{4D (\text{ierf}(1 - u))^2}, \quad (\text{B10})$$

where ierf is the inverse error function which can be solved for numerically in an efficient manner using the secant method. The set t_u are then drawn from the first-passage distribution.

The task of drawing from the distribution $P_2(t|r)$ shown in the bottom panel of Fig. 10 is readily accomplished by drawing a random number p uniformly on $(0, 1)$ and then solving the implicit equation $C_2(t_u|r) = p$ for the time t_u , where $C_2(t|r)$ is the cumulative distribution $C_2(t|r) = \int_0^t d\tau P_2(\tau|r)$. The cumulative distribution can be computed numerically by applying the Stehfest algorithm to form the inverse Laplace transform of $\tilde{C}_2(s|r) = \tilde{P}_2(s|r)/s$ (see bottom-most panel of Fig. 10).

¹B. Alberts, A. Johnson, J. Lewis, M. Raff, K. Roberts, and P. Walter, *Molecular Biology of the Cell*, 4th ed. (Garland, New York, 1994).

²I. Bahar and A. J. Rader, *Curr. Opin. Struct. Biol.* **15**, 586 (2005).

³G. A. Voth, *Coarse-Graining of Condensed Phase and Biomolecular Systems* (CRC, Boca Raton, 2008).

⁴S. Park and N. Agmon, *J. Phys. Chem. B* **112**, 5977 (2008).

⁵H. X. Zhou and A. Szabo, *Biophys. J.* **71**, 2440 (1996).

⁶B. J. Sung and A. Yethiraj, *J. Chem. Phys.* **123**, 114503 (2005).

⁷N. A. A. V. Popov, *Chem. Phys. Lett.* **340**, 151 (2001).

⁸H. Kim, M. Yang, and K. J. Shin, *J. Chem. Phys.* **111**, 1068 (1999).

⁹P. P. Schmidt, F. Tavers, and T. Barman, *Biochemistry* **34**, 824 (1995).

¹⁰R. D. Banks, C. C. F. Blake, P. R. Evans, R. Haser, D. W. Rice, G. W. Hardy, M. Merrett, and A. W. Phillips, *Nature (London)* **279**, 773 (1979).

¹¹B. E. Bernstein, P. A. M. Michels, and W. G. J. Hol, *Nature (London)* **385**, 275 (1997).

¹²B. E. Bernstein, D. M. Williams, J. C. Bressi, P. Kuhn, M. H. Gelb, G. M. Blackburn, and W. G. J. Hol, *J. Mol. Biol.* **279**, 1137 (1998).

¹³A. Geerlof, P. P. Schmidt, F. Tavers, and T. Barman, *Biochemistry* **36**, 5538 (1997).

¹⁴A. Geerlof, F. Tavers, T. Barman, and C. Lionne, *Biochemistry* **44**, 14948 (2005).

¹⁵A. Varga, J. Szabo, B. Flachner, P. Konarev, E. Graczer, J. Szabo, D. Svergun, P. Zavodszky, and M. Vas, *FEBS Lett.* **580**, 2698 (2006).

¹⁶A. Varga, J. Szabo, B. Flachner, Z. Guyolya, F. Vonderviszt, P. Zavodszky, and M. Vas, *FEBS Lett.* **583**, 3660 (2009).

¹⁷G. Auerbach, R. Huber, M. Grättinger, K. Zaiss, H. Schurig, R. Jaenicke, and U. Jacob, *Structure (London)* **5**, 1475 (1997).

¹⁸We model the enzymatic dynamics under conditions where the concentrations of enzyme and substrates are similar to those found in the cell. However, the cellular medium is crowded by other macromolecular species that can change the character of the protein structure and dynamics. See, for example, A. B. Fulton, *Cell* **30**, 345 (1982).

¹⁹C. Guilbert, F. Pecorari, D. Perahia, and L. Mouawad, *Chem. Phys.* **204**, 327 (1996).

²⁰N. Vaidehi and I. W. A. Goddard, *J. Phys. Chem.* **104**, 2375 (2000).

²¹E. Balog, M. Laberge, and J. Fidy, *Biophys. J.* **92**, 1709 (2007).

²²Z. Palmi, L. Chaloin, C. Lionne, J. Fidy, D. Perahia, and E. Balog, *Proteins* **77**, 319 (2009).

²³R. Inoue, R. Biehl, T. Rosenkrantz, J. Fitter, M. Monkenbusch, A. Radulescu, and D. Richter, *Biophys. J.* **99**, 2309 (2010).

²⁴M. M. Tirion, *Phys. Rev. Lett.* **77**, 1905 (1996).

²⁵P. Maragakis and M. Karplus, *J. Mol. Biol.* **352**, 807 (2005).

²⁶V. Tozzini, *Curr. Opin. Struct. Biol.* **15**, 144 (2005).

²⁷A similar network model was constructed for the enzymatic dynamics of adenylate kinase [C. Echeverria, Y. Togashi, A. S. Mikhailov, and R. Kapral, *Phys. Chem. Chem. Phys.* **13**, 10527 (2011)]; however, the conformational changes were induced by probabilistic changes in the potential function and the substrate and its dynamics were not included explicitly as in our model for PGK.

²⁸L. Zerrad, A. Merli, G. Schroder, A. Varga, E. Graczer, P. Pernot, A. Round, M. Vas, and M. Bowler, *J. Biol. Chem.* **286**, 14040 (2011).

²⁹J. L. Griffin, M. W. Bowler, N. J. Baxter, K. N. Leigh, H. R. Dannatt, A. M. Hounslow, G. M. Blackburn, C. E. Webster, M. J. Cliff, and J. P. Waltho, *Proc. Nat. Acad. Sci. USA* **109**, 6910 (2012).

³⁰See <http://www.molmovdb.org/cgi-bin/morph.cgi?ID=088521-3840> for morphing analysis of human form of phosphoglycerate kinase.

³¹A. Malevanets and R. Kapral, *J. Chem. Phys.* **110**, 8605 (1999).

³²T. Ihle and D. M. Kroll, *Phys. Rev. E* **63**, 020201 (2001).

³³T. Ihle and D. M. Kroll, *Phys. Rev. E* **67**, 066705 (2003).

³⁴R. Kapral, *Adv. Chem. Phys.* **140**, 89 (2008).

³⁵G. Gompper, T. Ihle, D. M. Kroll, and R. G. Winkler, *Adv. Polym. Sci.* **221**, 1 (2009).

³⁶N. Noguchi, N. Kikuchi, and G. Gompper, *Europhys. Lett.* **78**, 10005 (2007).

³⁷A. Malevanets and R. Kapral, *J. Chem. Phys.* **112**, 7260 (2000).

³⁸A. Malevanets and J. M. Yeomans, *Europhys. Lett.* **52**, 231 (2000).

³⁹N. Kikuchi, A. Gent, and J. M. Yeomans, *Eur. Phys. J. E: Soft. Matter Biol. Phys.* **9**, 63–66 (2002).

⁴⁰N. Kikuchi, C. M. Pooley, J. F. Ryder, and J. M. Yeomans, *J. Chem. Phys.* **119**, 6388 (2003).

⁴¹M. Ripoll, R. G. Winkler, and G. Gompper, *Eur. Phys. J. E* **23**, 349 (2007).

⁴²J.-X. Chen and R. Kapral, *J. Chem. Phys.* **134**, 044503 (2011).

⁴³R. Garrett and C. M. Grisham, *Biochemistry*, 3rd ed. (Brooks-Cole, Salt Lake City, 2004).

⁴⁴S. Minakami and H. Yoshikawa, *Biochem. Biophys. Res. Commun.* **18**, 345 (1965).

⁴⁵R. van Zon and J. Schofield, *J. Chem. Phys.* **128**, 154119 (2008).

⁴⁶M. Abramowitz and I. A. Stegun, *Handbook of Mathematical Functions with Formulas, Graphs, and Mathematical Tables* (Dover, New York, 1965).

⁴⁷A study of the effects of correlations on diffusion can be found in M. Ripoll, K. Mussawisade, R. Winkler, and G. Gompper, *Phys. Rev. E* **72**, 016701 (2005).

⁴⁸R. van Zon and J. Schofield, *J. Chem. Phys.* **132**, 154110 (2010).

- ⁴⁹G. Haran, E. Haas, B. K. Szpikowska, and M. T. Mas, [Proc. Natl. Acad. Sci. U.S.A.](#) **89**, 11764 (1992).
- ⁵⁰M. Wachsmuth, W. Waldemar, and J. Langowski, [J. Mol. Biol.](#) **298**, 677 (2000).
- ⁵¹M. Weiss, M. Elsner, F. Kartberg, and T. Nilsson, [Biophys. J.](#) **87**, 3518 (2004).
- ⁵²D. S. Banks and C. Fradin, [Biophys. J.](#) **89**, 2960 (2005).
- ⁵³G. Guigas, C. Kalla, and M. Weiss, [Biophys. J.](#) **93**, 316 (2007).
- ⁵⁴S. Redner, *A Guide to First-Passage Processes* (Cambridge University Press, Cambridge, 1991).
- ⁵⁵H. Stehfest, [Commun. ACM](#) **13**, 47 (1970).
- ⁵⁶H. Stehfest, [Commun. ACM](#) **13**, 624 (1970).